

2027
FR-5218
NRL Report 5218

CHARACTERISTICS OF RADAR SEA CLUTTER: OBSERVATIONS AT 220 MC

W. S. Ament, J. A. Burkett, F. C. MacDonald,
and D. L. Ringwalt

Wave Propagation Branch
Electronics Division

November 19, 1958



U. S. NAVAL RESEARCH LABORATORY
Washington, D.C.

APPROVED FOR PUBLIC RELEASE
DISTRIBUTION UNLIMITED

CONTENTS

| | |
|---|----|
| Abstract | ii |
| Problem Status | ii |
| Authorization | ii |
| INTRODUCTION | 1 |
| EQUIPMENT | 1 |
| SEA-CLUTTER MAGNITUDE AND VARIATION WITH RANGE AND GRAZING ANGLE | 1 |
| SWEEP-TO-SWEEP FLUCTUATION RATES AT FIXED RANGES | 2 |
| DISCUSSION | 3 |
| SUMMARY | 6 |
| REFERENCES | 6 |

ABSTRACT

Measurements of sea-clutter echo power and fluctuation characteristics have been made with a 220-Mc horizontally polarized radar mounted in a blimp. For well-developed sea conditions, with surface winds varying from 0 to 12 knots, there was little variation in σ_0 , the radar area per unit horizontal area of sea surface, as a function of azimuth. As a function of grazing angle θ , σ_0 varied as θ^4 over 1 to 14 deg, the range of the observations. Clutter fluctuation rates were generally higher when the radar looked crosswind than when it looked up or downwind. Crosswind echoes often contained well-defined periodic fluctuations at rates corresponding to twice the period of a classical ocean wave of half the radar's wavelength. The upwind echoes often fluctuated at high rates corresponding to the beat frequency between an echo from a stationary target and an echo from a wave crest moving at the dominant oceanographic crest speed.

PROBLEM STATUS

This is a final report on one phase of the problem; work is continuing on other phases.

AUTHORIZATION

NRL Problem R07-03
Projects NR 413-000, Task NR 413-002,
and NA 433-003
BuAer No. EL 43012

Manuscript submitted September 9, 1958

CHARACTERISTICS OF RADAR SEA CLUTTER: OBSERVATIONS AT 220 MC

INTRODUCTION

A novel opportunity to extend the knowledge of radar sea clutter to long wavelengths (136 cm) was presented when NRL obtained the use of a blimp-borne 220-Mc radar. This radar was designed by the Search Radar Branch, NRL, and installed by Goodyear Aircraft Company in the blimp (a modified ZPG-2W airship) for delivery (November 1957) to the Naval Air Development Unit, South Weymouth, Massachusetts for operations in this area. The Search Radar Branch held tests in abeyance; during November 1957, the Wave Propagation Branch of NRL installed recording equipment and, during seven flights generally ENE of Cape Cod, recorded about 30,000 ft of sea-clutter film. The flight altitudes were 500 and 3000 ft, and the grazing angles (angle between radar ray and mean sea plane) ranged from 1 to 14 deg. This report is based on preliminary samplings of the data.

The authors profited from discussions with Dr. E. W. Pike and Mr. James McGinn of MIT Lincoln Laboratory. In particular, illuminating discussions were held on the subject of removing receiver noise effects from the autocorrelation function, on the fit of measurements to a Gaussian spectrum, on the extrapolation of spectrum widths from centimeter wavelengths to the 200 to 400 Mc region (Pike and McGinn have collected sufficient data to cast serious doubt on a linear extrapolation), and on the possible need to measure the "range-element-to-range-element spectrum" (i-f) of sea clutter, as distinguished from the pulse-to-pulse spectrum, for fuller information on clutter physics.

EQUIPMENT

The basic parameters of the horizontally polarized NRL blimp-borne radar are:

| | |
|----------------------------|-----------------------|
| Frequency | 220 Mc |
| Pulse repetition frequency | 300 pps |
| Antenna dimensions | 33-1/2 by 9 ft |
| Antenna beamwidths | 9 deg by 28.6 deg |
| Transmitter power | 230 kw to 650 kw peak |
| Pulse width | 5 μ sec. |

The signals were recorded in two ways (Fig. 1)* with movie-camera photographs of an A-scope once per second (50-percent duty cycle), and with pulse-by-pulse recordings of the echo from single range elements. The pulse-by-pulse (P/P) scope has two channels, which are used to record two different range gates, separated from 1 μ sec to 5 μ sec in time (or range). From the correlation of the signals in these two gates, one obtains an estimate of whether or not the sea-clutter fluctuation frequencies "fill" the i-f passband. That they might not fill the band had been suggested in the phase measurements made by Lincoln Laboratory.

SEA-CLUTTER MAGNITUDE AND VARIATION WITH RANGE AND GRAZING ANGLE

The observed values of σ_o , the radar area per unit horizontal area of sea surface, are plotted against grazing angle θ in Figs. 2, 3, and 4. The elimination of the radar and

*All figures are found at the end of the report.

geometric parameters other than θ is accomplished through standard theory (1) using the radar parameters shown above; the absolute reference calibration was that obtained on the calibrating flight against a standard target at the Chesapeake Bay Annex of NRL. Allowance has been made for the vertical beam pattern of the antenna, which is fixed in elevation; the antenna heights are taken as 575 and 3075 ft to allow for the antenna's position relative to the blimp's altimeter. The correct values of σ_0 are considered to lie within +1.5 and -4.5 db of the plotted points, the uncertainty being due primarily to difficulties in the calibrating flight. The pulse-by-pulse film record from the calibrating flight had a reading error of ± 1.5 db, owing to video "pulling" of the base line. Further, the target echo varied only 12 to 15 db from lobe max to lobe min, as compared with 20 to 30 db in previous observations at 440 Mc from an airplane.

Except for two sets of points (which deviate for an unknown cause) on Nov. 12 (Fig. 2), the plotted values of σ_0 cluster well around a θ^4 straight line over 1 to 14 deg range of θ (i.e., where received power $P_R \propto R^{-7}$, it is assumed that $P_R \propto (h/R)^4 R^{-3} \approx \theta^4 R^{-3}$ and therefore $\sigma_0 \propto \theta^4$, where h = radar altitude). This behavior is considered to be due to the radar illumination of the important higher wave echoers (1), an illumination consisting of the wave direct from the radar and a wave reflected from a plane close to the mean-sea plane with reflection coefficient minus 1. It would be unsafe to extrapolate these curves to angles higher than 14 deg, since the 220-Mc illumination may deviate from this direct-plus-reflected mode. To extrapolate to other wavelengths is similarly unsafe owing to lack of precise knowledge as to the sea states existing during the measurements.

SWEEP-TO-SWEEP FLUCTUATION RATES AT FIXED RANGES

All of the data have been scanned visually; typical fluctuation rates observed on the raw pulse-by-pulse film varied from 1/3 cps to 5 cps, the most common observation being around 2.5 to 3 cps. The fluctuation data were ordinarily processed in the form of 20-lag autocorrelation functions. The autocorrelator is limited to a total input of 1000 pulses and an output for 21 values of τ (the pulse spacing), but it can be programmed to accept every pulse, every second pulse, or every fourth, eighth, sixteenth, or thirty-second pulse for 1000-pulse samples of greater length in real time. This is the reason for the various steps in τ in the correlograms. In some cases the subtotals for consecutive samples have been added to give long (time) samples for small values of τ . All of the correlations processed so far, except for a great many repetitious short samples on Nov. 7, appear in Figs. 5 to 15. These figures are ordered by date and azimuth with respect to wind; the altitudes and grazing angles appear on each figure.

From the samples analyzed so far, several different features have appeared.

1. The pulse-by-pulse films show occasional short bursts of high-frequency periodic components in the data. There is usually only one frequency visible at a given time, but this frequency can be from 7 to 24 cps. These bursts occur predominantly in the low-angle, low-altitude data. In the samples correlated so far, they are noticeable only in the upwind autocorrelation plots (Figs. 6, 9, and 13) to a degree depending on the amplitude of the burst and the ratio of burst length to sample length.
2. The rms fluctuation rate (a measure of the width of the spectrum of fluctuations) varies with wind speed. In the one case in which a comparison can readily be made, this rms value corresponds well with the ocean-wave velocity-difference spectrum (2).
3. The rms frequency tends to be higher in the crosswind data than in either the upwind or downwind data. This tendency is clearest for the most frequently observed

geometries (Figs. 13, 14, and 15). The log τ at which the correlation equals 0.5 is plotted in Fig. 16 for the data of Nov. 13. There is a clear frequency dependence on azimuth with respect to wind, but very little on grazing angle.

A nearly periodic component with a frequency around 3 cps appears quite regularly in the crosswind data but has not been observed yet at other azimuths (Figs. 8, 12, and 15).

Explanations of these fluctuation characteristics are believed to be as follows:

1. The high-frequency, periodic components are doppler difference frequencies between echoes from stationary (zero radial velocity) scatterers and from classical wind-wave velocities. The most probable conditions for seeing pure frequencies are at small grazing angles, when the echoes from individual wave crests are accentuated. This effect should be maximum at upwind azimuths, where the wave-crest lines are normal to the radar rays and have higher relative velocities.
2. The rms fluctuation rate of the echo (to be defined later) could be the result of the rms velocity difference for the entire spectrum of ocean waves generated at a given wind speed, but possible contributions by particle velocities and wind-blown crests are not ruled out by the data.
3. The low-frequency periodic component seen crosswind is twice the frequency of the "resonant" standing (ocean) wave, which has a wavelength equal to one-half the radar wavelength. A standing ocean wave of this wavelength acts as a grating with strong first-order scattering back to the radar; this grating appears and disappears with twice the frequency of vertical oscillation of a given ocean-surface element. The larger rms fluctuation rate seen crosswind is at times due to this periodic component but would normally be larger than the rms at other azimuths, due to the angular spectrum of the waves.

DISCUSSION

The Fleet Weather Central predictions of sea state were received daily throughout the test, and the predicted wave periods range from 4 to 8 seconds. For the three days under discussion here (Nov. 7, 12, and 13), the predicted periods were 6, 5, and 4 seconds, respectively. Classical ocean waves of these periods have velocities of 30, 25, and 20 ft/sec. These values correspond to beat frequencies (a wave-crest echo beating with an echo from a fixed target) of 14, 11.5, and 9 cps at 220 Mc. The observed winds for these days were:

| <u>Date</u> | <u>Wind Velocity</u> |
|-------------|---|
| Nov. 7 | 10 to 12 knots (sea fully developed) |
| Nov. 12 | calm to 8 to 10 knots, geostrophic wind 8 knots |
| Nov. 13 | calm to 8 or 9 knots. |

The predicted periods, as judged from the observed winds, are probably good estimates of the peak (most frequently observed) values. Hydrographic Office Publication 603, p. 48 (Ref. 2) gives seven seconds as a peak period for an 11 to 12 knot wind with waves of six-second period having about 1/10 of this maximum frequency of occurrence.

On an autocorrelation plot, a frequency f is shown by the appearance of a damped sine wave, given approximately by $A(\tau) \cos(2\pi f\tau)$, $A(\tau)$ decreasing with τ . Accordingly, the frequencies for these three days, in Figs. 6, 9, and 13, are judged to be 16, 15.4, and 9 cps, respectively. The first of these is subject to wide interpretation, because there is only one cycle on the plot, and the estimated distance from max to min of $\cos(2\pi f\tau)$ depends on the slope of the background "noise" correlation curve. The second frequency, 15.4 cps, comes from Fig. 10, which contains the same data as in Fig. 9, but with only every 16th

pulse read, so that 15.4 cps beats with the 18.75-cps sampling rate. With so few samples, even this much agreement with the wave velocities is somewhat fortuitous, since all doppler frequencies below the maximum should be possible. Such lower frequencies are observable by inspection of the film.

The following are taken as a summary of the rms fluctuation rates in Figs. 5 to 15:

| Date | Upwind (cps) | Crosswind (cps) |
|---------|---------------|-----------------|
| Nov. 7 | 1.8, 2.0, 2.2 | 1.6, 2.6 |
| Nov. 12 | 1.1, 1.2 | 1.2, 2.1 |
| Nov. 13 | 0.4 | 0.9 |

These data are extracted from only a few curves of Figs. 5 to 15, chosen because of their shape. Pike and McGinn (3) have shown how to remove the effect of receiver noise from the autocorrelation function, and the resultant curve (correlation computed in power units) should be parabolic (to two terms), the coefficient of the second term being the mean-square spectrum width ν^2 , defined as

$$\overline{\nu^2} = \frac{\int_0^{\infty} \nu^2 S(\nu) d\nu}{\int_0^{\infty} S(\nu) d\nu}$$

where $S(\nu)$ is the rf clutter spectrum shifted in frequency so that

$$\int_0^{\infty} \nu S(\nu) d\nu = 0.$$

The rms values given above are for the curves on which such a parabolic fit is reasonable; the tabulated data are believed representative for other samples on the given day.

The ocean-wave period distribution for an 11 to 12 knot wind given in Hydrographic Office Publication No. 603, p. 48 (Ref. 2), has been replotted in Fig. 17 in units of velocity; the computed velocity-difference distribution is also presented there. The standard deviation of this difference distribution is 5.1 ft/sec, or 2.3 cps at 220 Mc. Under the assumption that the wave velocity is also the radar scatterer velocity, this standard deviation of 2.3 cps is to be compared with the radar values of 1.8, 2.0, and 2.2 cps observed upwind on Nov. 7. Because conditions of light and variable winds are probably not ideal, and because H. O. Publication 603 (Ref. 2) does not give spectra for the lower wind speeds, the comparison has not been extrapolated to the other days.

This order-of-magnitude agreement of the radar doppler spectrum with the ocean-wave-velocity spectrum does not prove that the entire radar spectrum is due to gravity-wave velocities, because the velocity differences here are similar in magnitude to the velocity differences reported for radars of centimeter wavelengths (4), where the absolute scatterer velocities are of the order of 1 to 5 knots, more or less independent of wind speed. The rms spread (from 0.4 to 2.2 cps) is greater than normally reported for centimeter wavelengths. If the increase in rms value with increased wind speed continues in further analysis of the data, the hypothesis that the 220-Mc scatterers are gravity waves would be strengthened.

The theory that the low-frequency component could be the result of resonant standing waves is based on its occurrence crosswind, where waves travelling in opposite directions would more likely be generated and would probably be easier for the radar to see. For 220 Mc, the resonant wavelength would be 2.2 ft; running ocean waves of this length have a period of 0.65 sec, and standing waves form and re-form with periods of 0.33 sec. Hence the radar should see 3 cps. The values for Nov. 13 (Fig. 15) vary from 2.8 to 3.1 cps, and those for Nov. 12 span the same values. The Nov. 7 data give 2.8 cps; this number is probably low, because it is calculated from the first half-cycle of the autocorrelation curve. Because there are so few cycles in all these curves, various values can be deduced, but the ones quoted were obtained by using as many integral multiples of a half-cycle as could be found on the on the autocorrelation curve. If one stops counting on a maximum of the curve, the resultant frequency is too high, and if one stops on a minimum the resultant frequency is too low; this is an effect of the damping of the cosine wave. The frequencies of Fig. 15 cluster around 3 cps, with less scatter, percentagewise, than that observed for the high-frequency fluctuation rates.

There are of course two difficulties attached to attributing these results to standing ocean waves. One is that the amplitude of this wave is very small (classically less than 0.3 ft); the other is that the observed frequency of fluctuation should be invariant. With respect to amplitude, one can only add that there are about 1000 such waves ($\lambda = 2.2$ ft) in a pulse length. A qualitative oceanographic reason for variations in the observed frequency is that these small waves would be stretched or condensed when superposed upon a crest or trough of a long ocean wave. Hence the resonant 2.2-ft wavelength might have a period altered from the classical period, depending on position on the long wave pattern.

As a function of grazing angle θ , the resonant ocean wavelength varies as $\cos \theta$, so that there should be a possibly detectable systematic change in the resonant fluctuation rate with θ . On the other hand, at grazing angles, the echoes from wave crests dominate; here the resonant rates may be systematically changed by the preferred position of the resonant waves on the long wave pattern. Perhaps more importantly, wind dynamics and oceanographic nonlinearities should be specially important at wave crests, so that resonant regularities would be broken up there. Hence resonant periodicities should be more evident for the larger θ , where the regular structure in the troughs is visible. This conclusion is supported generally by the plots for Nov. 13 (Fig. 15) but is opposed by those for Nov. 12 (Fig. 12), oceanographic conditions being roughly the same. Hence, the relative importance of the effects discussed in this paragraph remains conjectural.

The expected larger rms value crosswind due to the angular spectrum is based upon the following example. Consider a single-frequency (and hence single-velocity) ocean wave with a probable direction distribution given by $\cos \phi d\phi$, where ϕ is the angle with respect to the wind vector ($|\phi| < 90$ deg). Then the upwind distribution of radial wave-crest velocities would be proportional to $v dv / \sqrt{1-v^2}$ in $0 < v < v_{\max}$, while crosswind the distribution would be flat, i.e., $C dv$ in $-v_{\max} < v < v_{\max}$. Thus crosswind shows a larger probability of large velocity differences, so that the greater rms value would be at crosswind, as observed.

It was found on the calibration flight at CBA that the antenna azimuth indicator (with respect to north) was in error by 30 to 40 deg. The indication was found correct early in the experiment, and when it deviated is not known. The most serious result of this is an increase in the observed fluctuation rates due to finite antenna beamwidth. There is some evidence within the data that the antenna pointing was correct for the data given here. The antenna is mounted in the gas bag, and the radiated power is attenuated in the tail and nose structures of the blimp. The antenna, pointed along the ground track, is pointed away from the nose structure by the ship's crab angle, hence the greater the crab angle, the greater the received signal. This effect has not been compensated for in Fig. 3 (Nov. 13) where, of the two crosswind points, the lower set is the result of confusion between heading and course resulting in the antenna's being pointed directly through the nose cone. This would

not have decreased the signal if the antenna pointing indication had been in error. The same kind of correlation with pointing is found in the Nov. 12 data (Fig. 2), where the up and downwind data (at ranges of 4, 2.2, and 1.2 miles) were taken through the nose cone.

SUMMARY

Measurements of sea-clutter echo power and fluctuation characteristics have been made with a 220-Mc horizontally polarized radar mounted in a blimp. For well-developed sea conditions, with surface winds varying from 0 to 12 knots, there was little variation in σ_0 , the radar area per unit horizontal area of sea surface, as function of azimuth. As a function of grazing angle θ , σ_0 varied as θ^4 over 1 to 14 deg, the range of the observations. Clutter fluctuation rates were generally higher when the radar looked crosswind than when it looked up or downwind. Crosswind echoes often contained well-defined periodic fluctuations at rates corresponding to twice the period of a classical ocean wave of half the radar's wavelength. The upwind echoes often fluctuated at high rates corresponding to the beat frequency between an echo from a stationary target and an echo from a wave crest moving at the dominant oceanographic crest speed.

REFERENCES

1. Katzin, M., "On the mechanisms of Radar Sea Clutter," Proc. I.R.E. 45:44 (1957)
2. Pierson, W.J., Neumann, G., and James, R.W., "Practical Methods for Observing and Forecasting Ocean Waves by Means of Wave Spectra and Statistics," Hydrographic Office Publication No. 603, 1955
3. McGinn, J.W., and Pike, E.W., "Theory and Procedure for Computing Moments of 'Clutter' Spectra from Sequences of Amplitude or Phase Measurements in Presence of Noise," to appear in Record of Symposium on Statistical Methods in Radio Wave Propagation, held at Univ. of Calif., June 18-20, 1958
4. Hicks, B.L., Knable, N., Kovaly, J.J., Newell, G.S., and Ruina, J.P., "Sea Clutter Spectrum Using Airborne Coherent Radar III," Univ. of Ill. Control Systems Laboratory Report R-105, May 1958

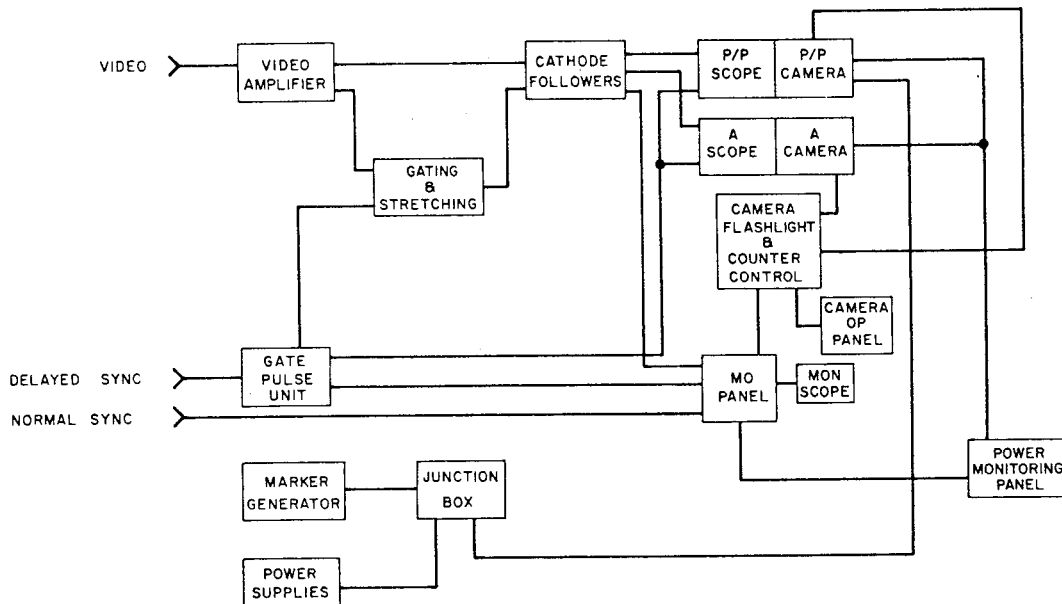


Fig. 1 - Block diagram of recording system

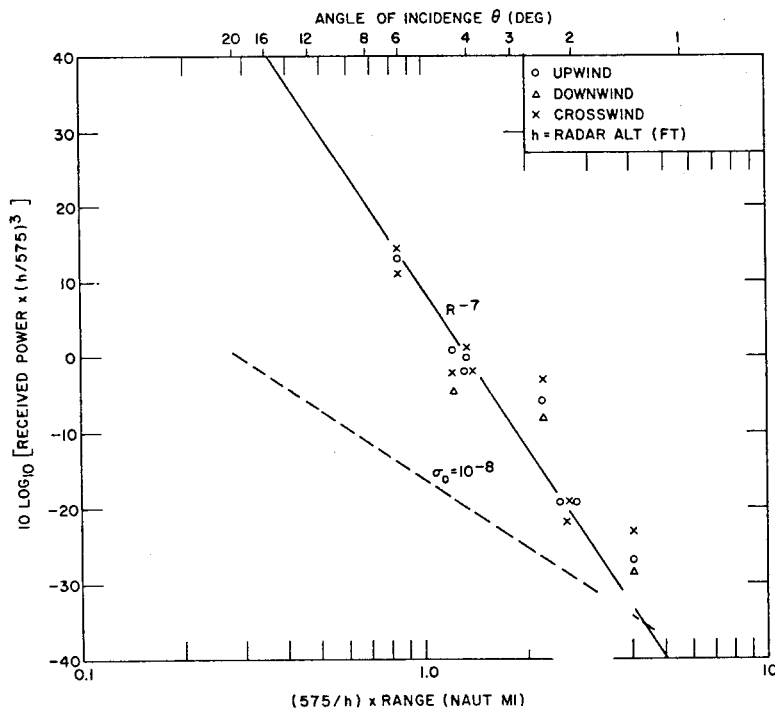


Fig. 2 - Received power, Nov. 12, 1957

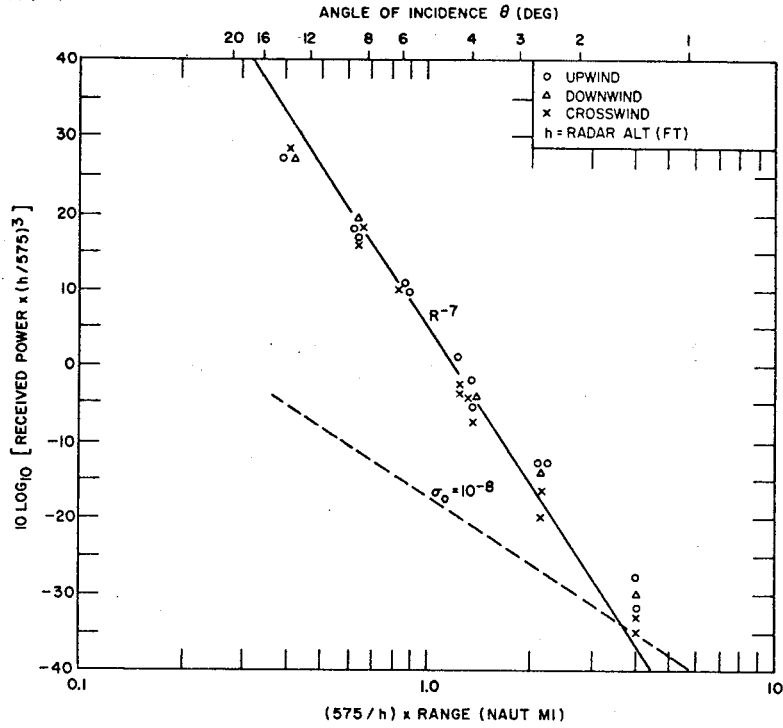


Fig. 3 - Received power, Nov. 13, 1957

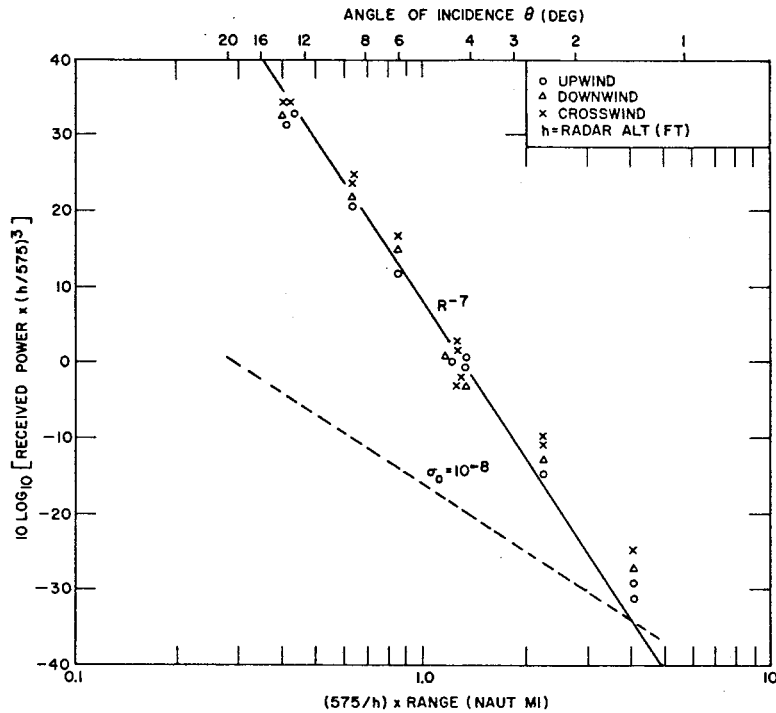


Fig. 4 - Received power, Nov. 14, 1957

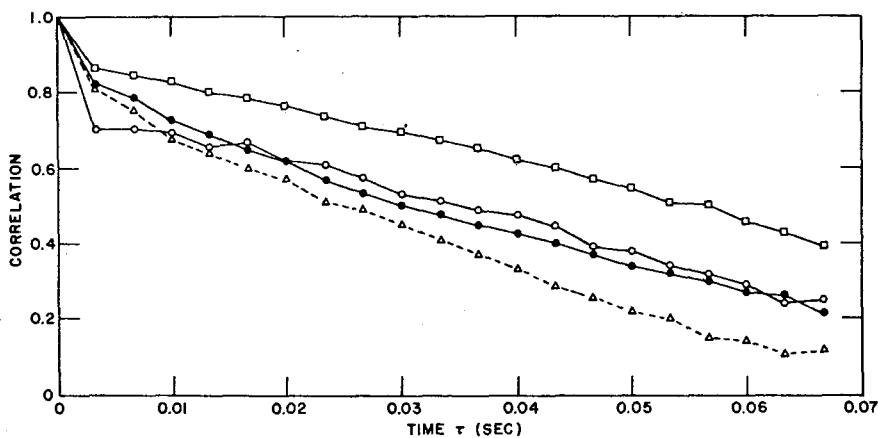


Fig. 5 - Sweep-to-sweep correlations at a fixed range, Nov. 7, 1957, upwind, 4 deg, 3000-ft altitude, 3-sec samples

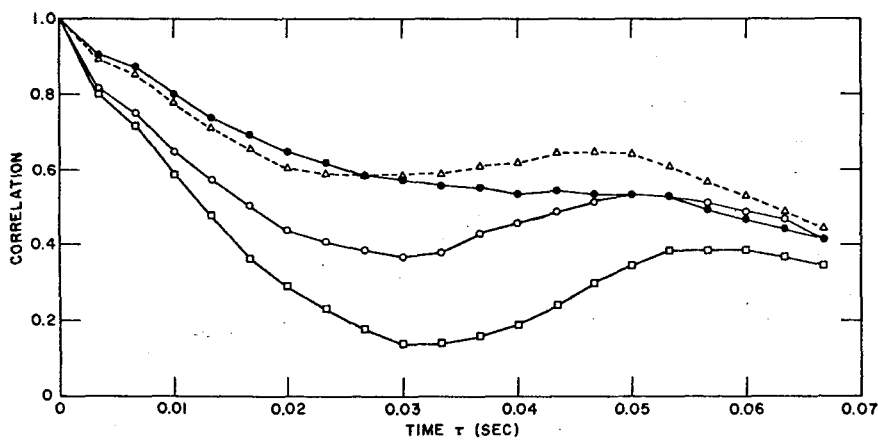


Fig. 6 - Sweep-to-sweep correlations at a fixed range, Nov. 7, 1957, upwind, 4 deg, 3000-ft altitude, 3-sec samples exhibiting a periodic component

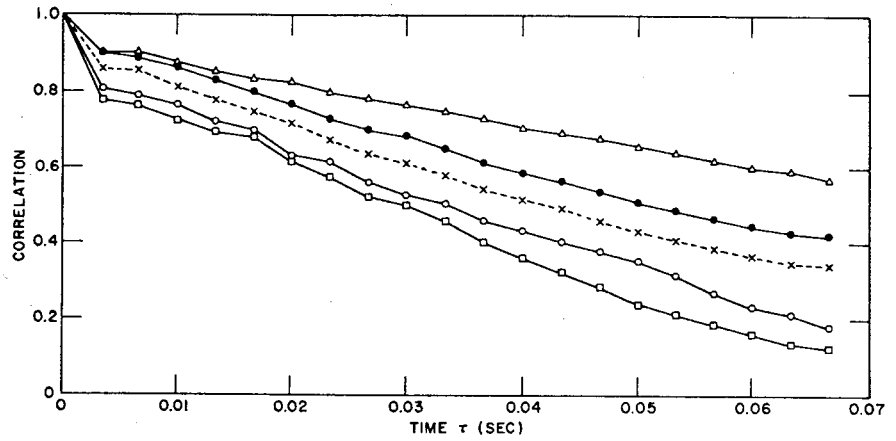


Fig. 7 - Sweep-to-sweep correlations at a fixed range, Nov. 7, 1957, crosswind, 4 deg, 3000-ft altitude, 3-sec samples

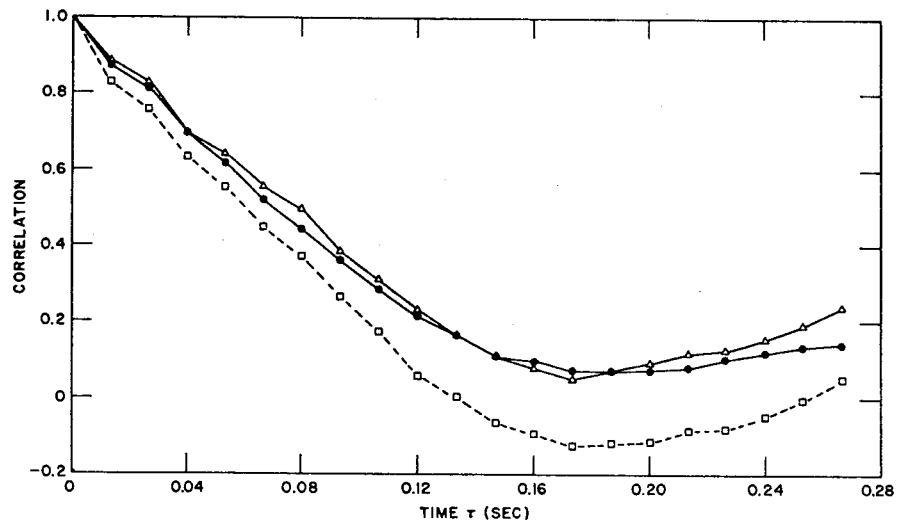


Fig. 8 - Sweep-to-sweep correlations at a fixed range, Nov. 7, 1957, crosswind, 6 deg, 3000-ft altitude, 13-sec samples

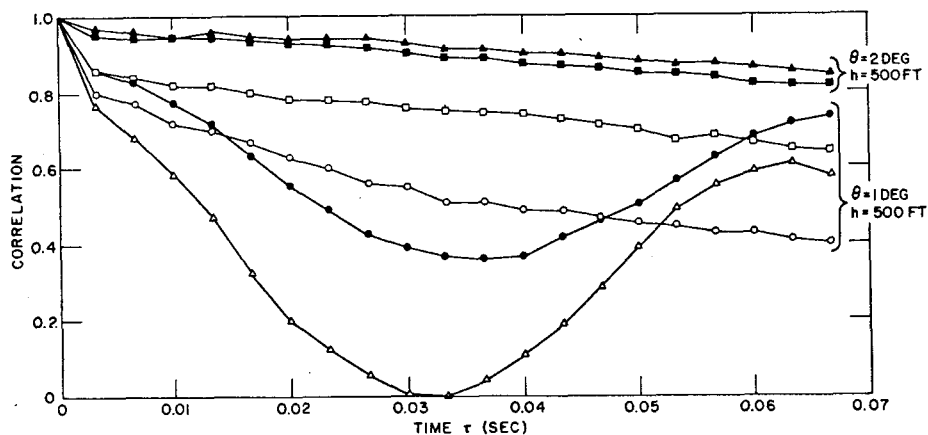


Fig. 9 - Sweep-to-sweep correlations at a fixed range, Nov. 12, 1957, upwind, 1 and 2 deg, 500-ft altitude, 26-sec samples

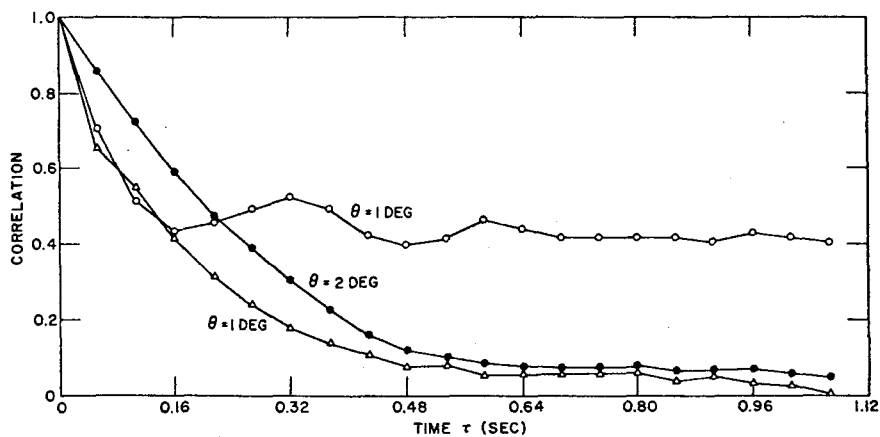


Fig. 10 - Sweep-to-sweep correlations at a fixed range, Nov. 12, 1957, upwind, 1 and 2 deg, 500-ft altitude, 53-sec samples

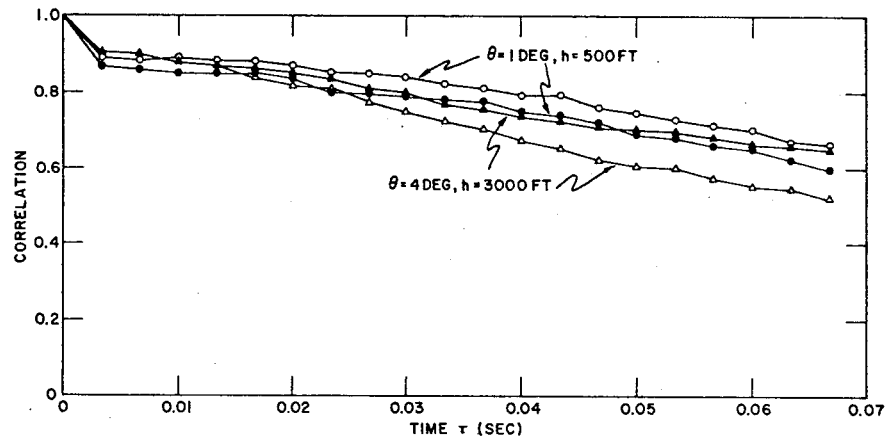


Fig. 11 - Sweep-to-sweep correlations at a fixed range, Nov. 12, 1957, crosswind, 1 and 4 deg, 500-ft and 3000-ft altitudes, respectively, 26-sec samples

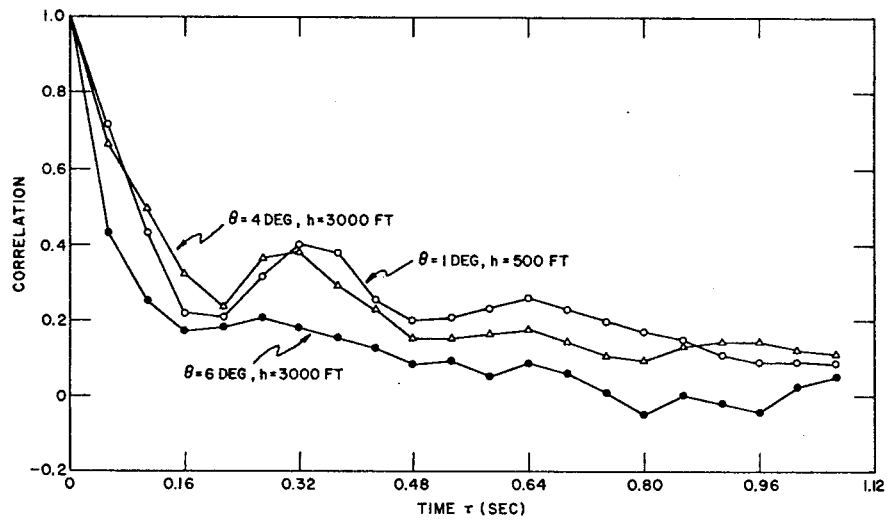


Fig. 12 - Sweep-to-sweep correlations at a fixed range, Nov. 12, 1957, crosswind, 53-sec samples

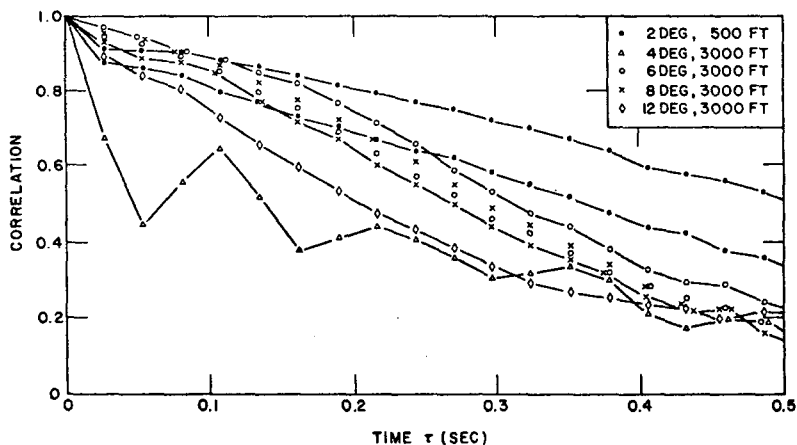


Fig. 13 - Sweep-to-sweep correlations at a fixed range, Nov. 13, 1957, upwind, 26-sec samples. Two sets of correlation points were left unconnected due to space limitations on the graph.

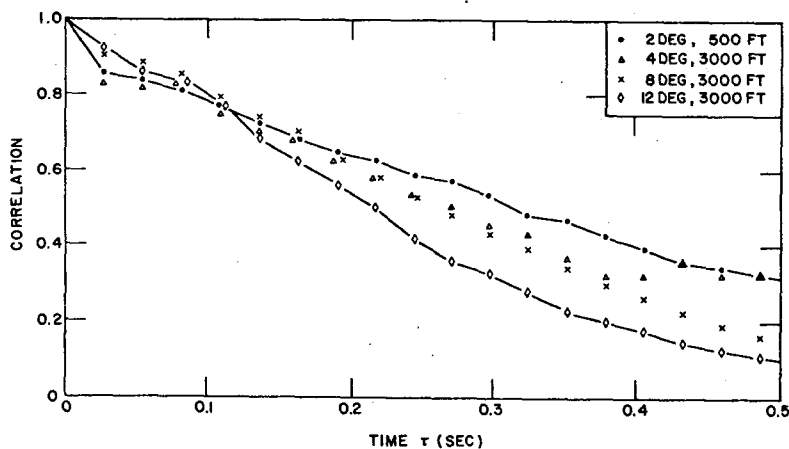


Fig. 14 - Sweep-to-sweep correlations at a fixed range, Nov. 13, 1957, downwind, 26-sec samples. Two sets of correlation points were left unconnected due to space limitations on the graph.

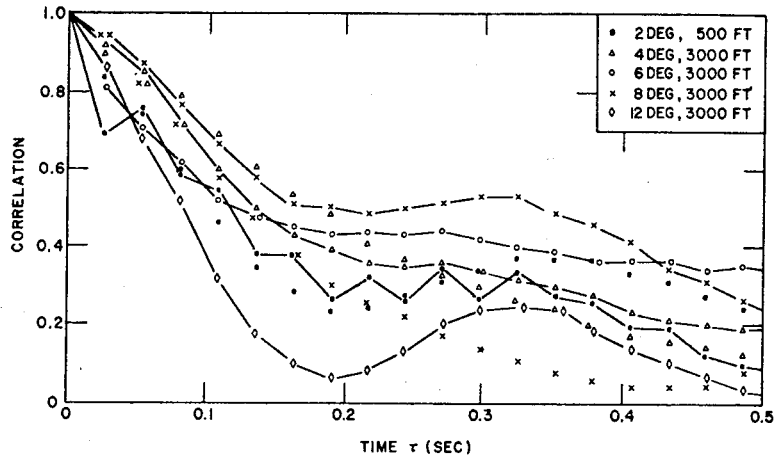


Fig. 15 - Sweep-to-sweep correlations at a fixed range, Nov. 13, 1957, crosswind, 26-sec samples. Two sets of correlation points were left unconnected due to space limitations on the graph.

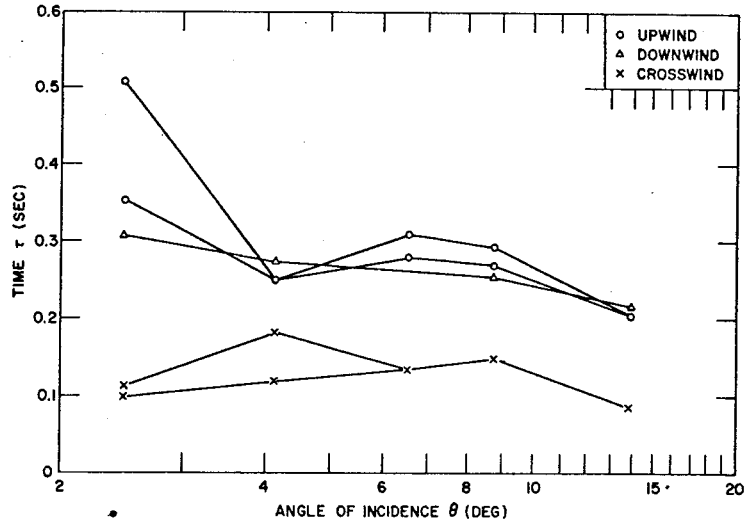


Fig. 16 - Time in which correlation decays to 0.5, Nov. 13, 1957

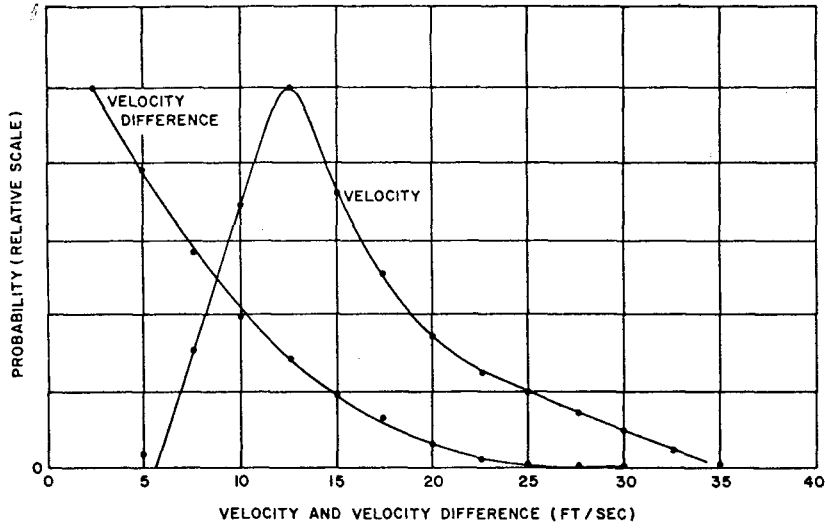


Fig. 17 - Distribution of ocean-wave velocities and velocity differences for an 11 to 12 knot wind

* * *